Received 5 April 2024; revised 20 May 2024; accepted 14 June 2024. Date of publication 4 July 2024; date of current version 1 August 2024.

Digital Object Identifier 10.1109/OJCOMS.2024.3423420

Optical Wireless 3-D-Positioning and Device Orientation Estimation

YIFAN HUANG [1], MAJID SAFARI [2] (Senior Member, IEEE), HARALD HAAS [3] (Fellow, IEEE), AND IMAN TAVAKKOLNIA [3] (Member, IEEE)

[1]Electronic and Electrical Engineering Department, University of Strathclyde, G1 1XQ Glasgow, U.K.

[2]Institute for Digital Communications, University of Edinburgh, EH9 3JW Edinburgh, U.K.

[3]Electrical Engineering Division, University of Cambridge, CB3 0FA Cambridge, U.K.

CORRESPONDING AUTHOR: Y. HUANG (e-mail: yifan.huang.2019@uni.strath.ac.uk)

This work was supported in part by the Project REASON, a U.K. Government funded Project through the Future Open Networks Research Challenge (FONRC) sponsored by the Department of Science Innovation and Technology (DSIT), and in part by the Engineering and Physical Sciences Research Council (EPSRC) through the Terabit Bidirectional Multi-User Optical Wireless System (TOWS) for 6G LiFi under Grant EP/S016570/1 and through the Platform for Driving Ultimate Connectivity (TITAN) under Grant EP/X04047X/1 and Grant EP/Y037243/1.

ABSTRACT Accurate sensing and localisation are considered as necessary features of future communication systems, including 6G. To harness the full potential of radio frequency (RF) and optical wireless communication (OWC), the localisation of user devices is essential, which further facilitates efficient beam steering, handover, and resource allocation. In this paper, we have considered a practical scenario where users are mobile with random device orientation. A convolutional neural network (CNN) is introduced to estimate the user position and orientation based on the received signal strength (RSS). CNN demonstrates superior performance in optical wireless positioning by proficiently extracting features from only RSS data. According to the simulation results it is observed that, by adjusting the structure of the dataset, a significant improvement in the estimation of the location is obtained in comparison with previous methods. We also consider having the noisy orientation data from the device sensors and investigate localisation performance in such a scenario. Finally, the impact of configuration of access points (APs) on the model is studied. This work demonstrates that a low-complexity accurate localisation, with average error as low as 1.8 cm, is indeed feasible.

INDEX TERMS LiFi, 6G, indoor positioning, transceiver, access point distribution.

I. INTRODUCTION

WITH the increasing demand for connectivity, communication technologies are rapidly evolving to provide high data rates, extremely low latency, and extensive coverage [1]. The Internet of Things (IoT) technology has also seen exponential growth in recent years. This means that we not only need to make significant breakthroughs in data capacity, but also focus on the critical needs that arise in IoT and other relevant services, such as sensing and positioning [2]. Global Navigation Satellite System (GNSS) uses satellite radio navigation technology to determine the spatial location and timing of targets [3]. The Global Positioning System (GPS) was the first operational GNSS and is the most widely used system globally. It relies on satellites continuously transmitting signals to ground receivers which use signal characteristics to calculate distances and positions, enabling accurate navigation and measurement operations [4]. However, GPS positioning accuracy is greatly degraded in indoor settings due to strong fading and shadowing effects. Therefore, utilising indoor communication systems for positioning has emerged as a promising approach, simultaneously offering communication and sensing capabilities [5], [6]. The accuracy of WiFi, cellular, and Bluetooth indoor positioning systems are generally low in indoor environments due to multi-path and other physical effects. A deep review of various localisation techniques is presented in a recent study [7].

TABLE 1. The comparison between DL-based VLP system.

Network	Space	Size	Positioning error	Remark
Weighted K-Nearest Neighbors [14]	2D	$5 \times 5 \times 3$ (m)	3.4 cm	2D positioning with single-directional structure
Supervised Learning [15]	2D	$4 \times 4 \times 2.5$ (m)	3.5 cm	2D positioning and 25 Transmitters
DNN [16]	2D	$5 \times 5 \times 3$ (m)	1.662cm	2D positioning and high complexity on computation
Two layer Artificial Neural Networks (ANNs) [17]	3D	$0.9 \times 1 \times 0.4$ (m)	less than 1 cm	small room size
ANNs [18]	3D	$5 \times 5 \times 3$ (m)	10.53 cm	Position and orientation estimation with single-directional structure

Optical wireless communication and light-fidelity (liFi) are high performance communication systems benefiting from unique features of light waves [8]. In this field, various optical wireless positioning systems are being proposed, generally showing superior localization performance compared to radio technologies. According to [9], a spatial modulation (SM)-based positioning algorithm achieves high accuracy of both 2-dimensional (2D) and 3-dimensional (3D) localisation, e.g., an average of 2.8 cm for a 3D localisation at a signal-to-noise ratio (SNR) of 30 dB. These results suggest that the algorithm performs exceptionally well in an idealized environment and a specific movement type. However, it is important to note that this work does not account for random orientation and achieving the assumed high SNR is challenging in practical scenarios. Furthermore, in [10], a low-complexity, time-difference-of-arrival (TDOA)-based indoor visible light positioning system utilizing an enhanced cross-correlation localization scheme was proposed and validated through experiments. The system demonstrates an average positioning accuracy of 9.2 cm within relatively small area of a 1.2×1.2 m^2 area at a height of 2 m.

However, conventional visible light communication (VLC) localization techniques often encounter multiple local minima challenges and necessitate supplementary data like initial positioning, pre-estimated orientation, or extra infrastructure alongside iterative algorithms [11], [12], [13].

Deep learning approaches have also been used for accurate positioning. Table 1 lists some of the most relevant works which use deep learning techniques. In [14], [15], [16], the positioning error was estimated in a 2D range, considering movement only in X-Y plane, but the model in this paper will consider the 3D range of the movements, more closely reflecting real-world scenarios. The model in [17] consider a small room of size by $0.9 \times 1 \times 0.4$ m, while this paper assume a room size of $5 \times 5 \times 3$ m. In [18], the authors addressed the challenge of estimating the 3D position and orientation of user equipment (UE) with single photodiode (PD) structure in an indoor LiFi systems, without prior knowledge of emission power. The average position error was 10.53 cm. CNNs excel in complex environments of optical wireless systems, processing all the physical effects of the environment and spatial light distribution effectively, even in dynamic, obstructed settings. One of the significant advantages of CNNs is their ability to extract meaningful features from the data, including those components traditionally considered as noise or imperfections. Moreover, CNNs can potentially adapt to new environments and reduce the need for re-calibration.

In this paper, we introduce a novel method that employs deep learning techniques, specifically artificial neural networks (ANNs), to enhance estimation accuracy. We use a multi-directional transceiver structure for the UE, featuring pairs of LED/PDs on the top side of the screen and three additional pairs on the other three sides. This is a promising structure which provides enhanced performance in the presence of random device orientation [19]. The CNN model in [18], cannot be used directly for positioning with a multi-directional transceiver. Our initial tests showed a performance degradation, even with multiple transceivers. In order to improve the performance for the multi-directional structure, a new CNN model is developed for estimating both position and orientation. Additionally, we consider a new datasets structure, using orientation information as feature vectors while focusing on the position estimation. This represents a scenario where orientation data is available from sensors of the device. The UE orientation information is measured via the phone sensor and recorded via software. This data is affected by noise from various sources and thus have an impact on the positioning accuracy. We further proposed a simple noise reduction algorithm for the training phase which reduced the impact of noise. The study also examines various number of APs for the system. Simulations indicate that the positioning error is 1.81cm with 16 APs in a noise-free environment, and 2.31cm in the noisy scenario. Notably, with the system simplified to a low-cost and low-complexity APs configuration, the current model continues to demonstrate robust performance. Our results show that a CNN-based positioning algorithm can achieve a low error in the range of 2 cm which is remarkable when compared to radio positioning systems.

The remainder of the paper is organized as follow. Section II introduces the system model which includes typical indoor LiFi model. Section III describes the deep learning framework. Finally, Sections IV and V discuss the simulation results and conclusion respectively.

II. SYSTEM MODEL

In this section, we present the system model including the environment, transceiver structure, channel model, random orientation model, and the received signal strength (RSS) analysis.

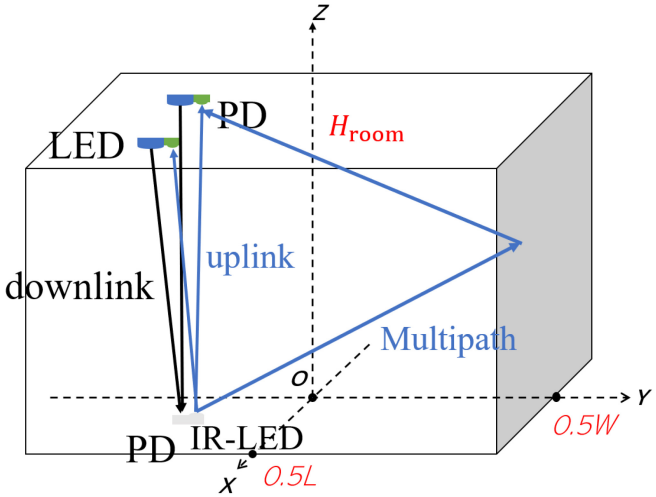

FIGURE 1. The typical visible light positioning system.

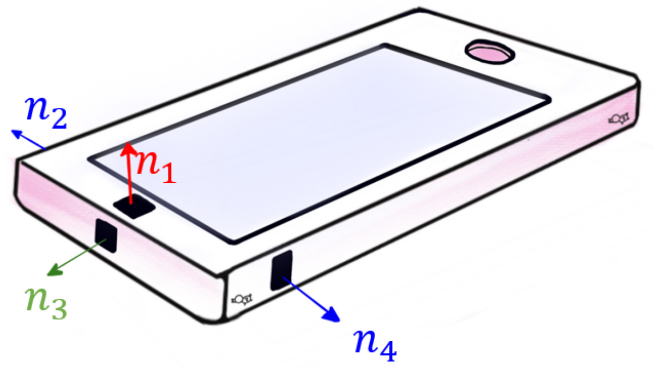

FIGURE 2. MDT structure for User Equipment.

A. SYSTEM SETUP

The layout of the LiFi system inside the room is depicted in Fig. 1. The dimensions of the room are denoted as $L \times W \times H_{\text{room}}$, respectively, representing the length, width and height of the room. APs are installed on the ceiling, each facing the floor. Each AP comprises an LED and a PD in close proximity to one another. The LEDs in the APs are utilized for illumination and data transmission, while the PDs are responsible for data reception. The UE is equipped with Infrared (IR)-LEDs and suitable PDs. As demonstrated in [19], having multiple receivers on different sides of UE can enhance the communication performance. Thus, adopting this concept, we consider the structure comprising multiple pairs of LED/PD, as illustrated in Fig. 2. LED/PD transceiver pairs are commercially available to be integrated in small UEs, such as the 'Light Antenna ONE' developed by pureLiFi [20], which is notably compact, with a size of only 14.5mm. The multi-directional transceiver (MDT) design integrates pairs of LED/PDs on top of the screen, with three additional pairs positioned on the remaining sides of the UE. The downlink is facilitated by the AP's LED, transmitting data in the visible light spectrum to the PD on the UE, while the uplink is realised through UE's IR-LED, transmitting the IR spectrum with the PD on the AP responsible for signal detection and reception. This configuration is strategically designed to address challenges frequently encountered in practical environments, such as obstructions, limited field of view (FOV), and the random position and orientation of the UE. By using each of the four IR-LED/PD pairs, the MDT structure can significantly reduce the impact of mentioned issues. In the assessment of RSS, the aggregate of the signal intensities from four IR-LED/PD pairs is calculated irrespective of the UE's position and orientation.

B. CHANNEL MODEL

We primarily focus on the uplink for the purpose of UE localisation and consider the intensity modulation direct detection (IM/DD) approach. As depicted in Fig. 1 and Fig. 2, the system has $N_{\text{t}} = 1$ or 4 IR-LEDs as transmitter elements. In addition, there are N_{r} PDs on the ceiling functioning as receive elements. In this paper, we investigate the impact of varying the number of access points (APs). Here, N_{r} represents the variable number of APs, which includes values of 4, 5, 8, and 16. The channel model can be succinctly expressed as

$$y = \mathbf{H}x + n, \tag{1}$$

where x represents the transmitted signal vector with dimensions $N_{\text{t}} \times 1$. The vectors y and n correspond to the received signal vector, also $N_{\text{r}} \times 1$ in length, and noise vector at each PDs, respectively. The noise in the current system is assumed to be real-valued additive Gaussian white noise, encapsulating all potential noise sources, such as shot noise and thermal noise, denoted as $n \sim \mathcal{N}(0_{\text{N}_\text{r}}, \sigma_n^2 I_{\text{N}_\text{r}})$. The variance of noise is expressed as $\sigma_{\text{n}}^2 = N_0 B$ where N_0 denotes the single-sided power spectral density of the noise, and B represents the bandwidth. The channel matrix $\mathbf{H}$ is detailed below:

$$\mathbf{H} = \begin{pmatrix} h_{1,1} & h_{1,2} & \cdots & h_{1,N_t} \\ h_{2,1} & h_{2,2} & \cdots & h_{2,N_t} \\ \vdots & \vdots & \ddots & \vdots \\ h_{N_r,1} & h_{N_r,2} & \cdots & h_{N_r,N_t} \end{pmatrix} \tag{2}$$

The element $h_{i,j} (i = 1, \ldots, N_{\text{r}},\ j = 1, \ldots, N_{\text{t}})$ in the channel matrix represents the gain of the link between the j^{th} UE transmitter and i^{th} PD. This gain can be calculated as follow:

$$h_{i,j} = h_{i,j}^{\text{LOS}} + h_{i,j}^{\text{NLOS}} \tag{3}$$

The equation indicates that the channel gain is the sum of the Line-of-Sight (LOS) channel gain and Non-Line-of-Sight (NLOS) channel gain. The distance d between transmitter and receiver pairs, and the orientation of the UE determines the LOS channel gain. The geometry of uplink channel model is shown in Fig. 3. As illustrated in the left of Fig. 3, the channel model geometry for LOS in i_{th} AP and j_{th} LED pairs is demonstrated. Φ refers to the half-power semiangle of LEDs; $\phi_{i,j}$ represents the radiance angle of LEDs, which

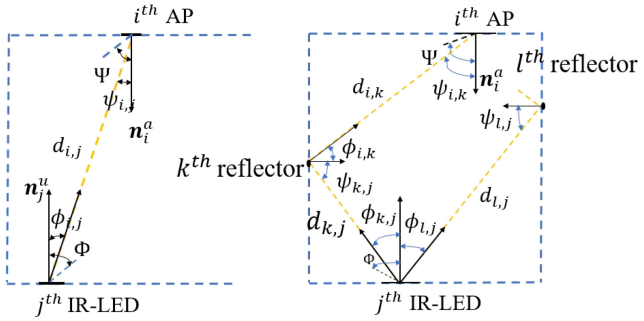

FIGURE 3. Uplink channel model geometry of indoor LiFi system.

is essentially the angle between the vector transmitter (Tx) - receiver(Rx) and the normal vector of LEDs; whereas, at the AP side, Ψ stands for the FOV of PDs on the AP; and $\psi_{i,j}$ is the angle of incidence at the receiver side. With the above orientation and position parameters, the LOS channel gain can be calculated by

$$h_{i,j}^{\mathrm{LOS}} = \frac{(m+1)A}{2\pi d_{i,j}^2}\cos^m(\phi_{i,j})\mathrm{rect}\left(\frac{\phi_{i,j}}{\Phi}\right)\cos(\psi_{i,j})\mathrm{rect}\left(\frac{\psi_{i,j}}{\Psi}\right) \tag{4}$$

where m represents the Lambertian emission order of LEDs which could be obtained as $m = -1/\log_2(\cos(\Phi_{1/2}))$, where the $\Phi_{1/2}$ is the half-power semiangle. The parameter A in (4) refers to the area of PD. In the case of the NLOS channel model, frequency domain analysis is utilised, which can take into account an infinite number of reflections, thereby enabling the accurate determination of the diffusion link, as noted by [21]. It is common to segment the indoor environment into small-area surface elements capable of reflecting light beams. These planar elements are assumed to have a FOV of 90° and a Lambertian order $m = 1$. Assuming the entire indoor model comprises N such elements, and considering the case of infinite number of reflections between i_{th} AP and j_{th} LEDs, the channel gain $h_{i,j}^{\mathrm{NLOS}}$ of the NLOS can be expressed as

$$h_{i,j}^{\mathrm{NLOS}} = \mathbf{r}^{\mathrm{T}}\mathbf{G}_\zeta\left(\mathbf{I} - \mathbf{E}\mathbf{G}_\zeta\right)^{-1}\mathbf{t} \tag{5}$$

where the vector $\mathbf{t}$ represents the link between LEDs and the surface elements in the indoor system, while the link between the surface of room and the i_{th} PDs on the APs is given as $\mathbf{r}$. The matrix $\mathbf{G}_\zeta$ describes the reflectivity of all the reflective surface elements, where $\mathbf{G}_\zeta = \mathrm{diag}(\zeta_1, \ldots, \zeta_N)$. The matrix $\mathbf{E}$, having the dimensions of $N \times N$, represents the LOS link transfer function for the surface elements, and the matrix $\mathbf{I}$ is an identity matrix of order N in the equation.

C. RANDOM ORIENTATION MODEL

Some devices such as smartphones, are capable of obtaining their corresponding 3D angles through a sensor and record angles using corresponding software. These angles can be interpreted as rotation angle for the initial coordinates, which include yaw (α), pitch (β), and roll (γ). As shown in the figure, these represent the rotation of the UE around the z-axis, x-axis, and y-axis, respectively. Depending on the actual use case, the range of yaw angle extends from 0° to 360°, the pitch angle varies from −180° to 180°, and the roll angle fluctuates from −90° to 90°. In accordance with Euler's rotation theorem, the rotation matrix can be denoted as $\mathbf{R} = \mathbf{R}_\alpha\ \mathbf{R}_\beta\ \mathbf{R}_\gamma$, where R_α,$\mathbf{R}_\beta$ and $\mathbf{R}_\gamma$ are shown in eq. (6) below.

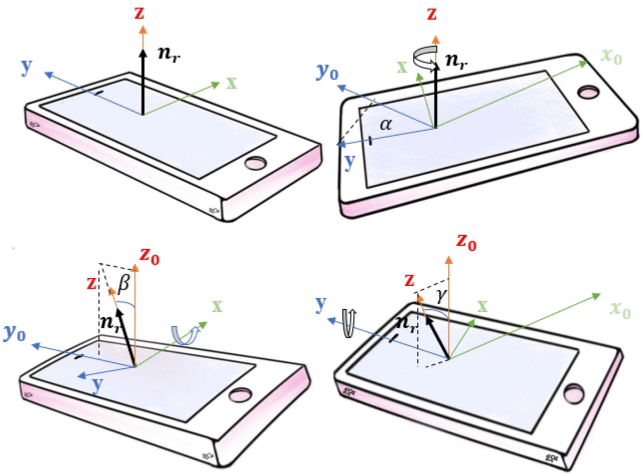

FIGURE 4. Orientation angle of user equipment: (a) normal coordinate; (b) yaw rotation angle on z-axis; (c) pitch rotation angle on x-axis; (d) roll rotation angle on y-axis.

Following the rotation matrix, the normal vectors $\mathbf{n}_j^{\mathrm{u}}$ of all the LEDs can be modified by $\mathbf{n}_j^{\mathrm{u}} = \mathbf{R}\mathbf{n}_0$, where $\mathbf{n}_0$ represents the initial state of the normal vector. The stochastic distribution of orientation angles (α, β, γ) are fitted as truncated Laplace distribution as described in [19].

$$\mathbf{R}_\alpha = \begin{bmatrix} \cos(\alpha) & -\sin(\alpha) & 0 \\ \sin(\alpha) & \cos(\alpha) & 0 \\ 0 & 0 & 1 \end{bmatrix},$$
$$\mathbf{R}_\beta = \begin{bmatrix} 1 & 0 & 0 \\ 0 & \cos(\beta) & -\sin(\beta) \\ 0 & \sin(\beta) & \cos(\beta) \end{bmatrix},$$
$$\mathbf{R}_\gamma = \begin{bmatrix} \cos(\gamma) & 0 & \sin(\gamma) \\ 0 & 1 & 0 \\ -\sin(\gamma) & 0 & \cos(\gamma) \end{bmatrix} \tag{6}$$

D. RECEIVED SIGNAL STRENGTH (RSS) ANALYSIS

In [18], RSS analysis was implemented to estimate the orientation and position of UE. In this estimation system, in order to obtain a more accurate 3D position and orientation, a reference signal needed to be transferred to the APs on the ceiling via the UE. We consider both communication and positioning functions, aligning closely with the realistic application scenarios. Consequently, the APs and UEs within the system comprise LED/PD pairs. The channel transmitting from the LED at the AP to the PD at the UE is designated as the downlink, primarily utilized for communication purposes. Conversely, the channel from the IR-LED at the UE to the

PD at the AP is defined as the uplink and is employed for both communication and positioning purposes. We only study positioning in this work. Building upon this concept, our approach involves the utilization of pulse-amplitude modulation (PAM) of order M. Consequently, the signal transmitted by LEDs can be considered equivalent to one of the M-PAM intensities, expressible as $I_m = \frac{2I}{(M+1)}m$ for $m \in [\,0, M-1\,]$, where I is the mean optical power emitted [2]. The received vector of signals at the i_{th} AP is then determined by substituting the channel gain matrix and input signals s into to eq. (1), resulting in $y_i = (\lambda \sum_{j=1}^{N_t} h_{i,j})s + n_i$, where λ denotes the PD responsivity. The SNR received at the i_{th} APs side is thus calculated as

$$\rho_i = \frac{\left(\lambda \sum_{j=1}^{N_t} h_{i,j}\right)^2 P_{elec}}{\sigma_n^2} \tag{7}$$

where the P_{elec} in the equation represents the electrical power of the transmitted signal s, given by $P_{elec} = \frac{I_{DC}^2}{3}\frac{M-1}{M+1}$. These equations allows us to derive the corresponding SNR from the channel gain and the variance of the noise in the channel. Each AP can have a distinct SNR value, leading to an SNR vector of $N_r \times 1$ dimensions as $\rho = [\rho_1, \rho_2, \ldots, \rho_{N_r}]$. SNR values are dependent on channel gains, which are influenced by the position and orientation of the UEs. Thus, each SNR vector correlates with a specific device position (x,y,z) and a orientation (α, β, γ).

III. RSS-BASED DEEP LEARNING MODELS FOR 3D POSITION ESTIMATION

Conventional positioning techniques, such as using time-of-arrival (TOA), require the precise measurement of signal travel time from the UE to various receivers. Additionally, these methods may depend on a predefined awareness of the signal's transmission power. However, deep learning-based approaches obviates these prerequisites by autonomously learning to interpret and analyze the characteristics of positioning signals directly from the collected data, thereby eliminating the dependency on pre-existing positional or power level information. In [18], it was demonstrated that ANNs in deep learning can be effectively applied to estimate the position and orientation of UE. From simulation results comparing CNNs with Multilayer Perceptrons (MLPs), we learned that models employing CNNs achieve higher estimation accuracy compared to those using MLPs. The following sections will detail the data set generation and the implemented deep learning framework.

A. DATASETS GENERATION

Each UE is randomly located within the indoor environment. Without loss of generality, its random distribution can be regarded as a uniform distribution, allowing the probability density functions (PDFs) of 3D position (x,y,z) of the UEs to be expressed as

$$f_x(x) = \frac{1}{L}\mu_{\left[-\frac{L}{2},\frac{L}{2}\right]}(x), \tag{8a}$$

$$f_y(y) = \frac{1}{W}\mu_{\left[-\frac{W}{2},\frac{W}{2}\right]}(y), \tag{8b}$$

$$f_z(z) = \frac{1}{H_{\text{devices}}}\mu_{[0,H_{\text{devices}}]}(z), \tag{8c}$$

where H_{device} is in the range of $0 < H_{\text{devices}} < H_{\text{room}}$. For the orientation datasets, we use the empirical distributions from [22] to achieve a highly accurate, measurement-based orientation datasets (α, β, γ). The UE rotation angles, recorded as yaw angle α, pitch angle β, and roll angle γ, are fitted as truncated Laplace distribution with mean and standard deviation represented as $(\mu_\alpha, \sigma_\alpha) = (\Omega - 90°, 3.67°)$, $(\mu_\beta, \sigma_\beta) = (40.78°, 2.39°)$ and $(\mu_\gamma, \sigma_\gamma) = (-0.84°, 2.21°)$ respectively [19]. In this context, Ω expresses the direction that the user faces when seating or moving. From a statistical aspect, the movement direction angle Ω can be treated as following the uniformly distribution in $[0°, 360°]$. To generate a target dataset of size N, the following steps are necessary: the position of the user's device is sampled with a uniform distribution function, and Ω is defined to generate the movement directional angles, thereby establishing the orientation of the UEs. Based on the previously calculated channel matrix $\mathbf{H}$, the SNR vector ρ derived from $\mathbf{H}$ can also be obtained. As such, two forms of datasets need to be generated. The first, named Position and Orientation estimation Dataset, estimates the position and orientation from the feature of SNR vectors. Here, the SNR vectors ρ, derived as described above, will be used as feature vectors, and the corresponding 3D position and 3D orientation will be labeled as $(x, y, z, \alpha, \beta, \gamma)$, as shown in Fig. 5(a). The second dataset is named Orientation-aided positioning Dataset, for which the emphasis is on the 3D position of user equipment (UE), with orientation data (α, β, γ) obtained from other sources, e.g., smart device sensors. This dataset uses SNR vectors ρ and orientations as inputs, with the position (x, y, z) as the CNN output, serving as labels for accurate UE positioning. Details are depicted in Fig 5(b). The primary rationale for generating two datasets is to reduce the complexity of the method and avoid unnecessary orientation estimation.

B. CNN MODEL IMPLEMENTATION

The primary objective is to identify a CNN with optimal parameters for extracting features from input vectors. Essentially, CNNs are networks designed to map and train continually, seeking the optimal parameters of CNN through comparison with a prediction error matrix.

The main training approach involves using corresponding feature vectors, either Position and Orientation estimation Dataset or Orientation-aided positioning Dataset and along with their labels, to instantaneously capture and extract features. This process aims to minimize the final loss function before saturation. A typical CNN will consist of several different layers: the input layer, convolutional layer, Rectified Linear Unit (ReLU) layer, pooling layer, and fully connected (FC) layer. By stacking these layers sequentially,

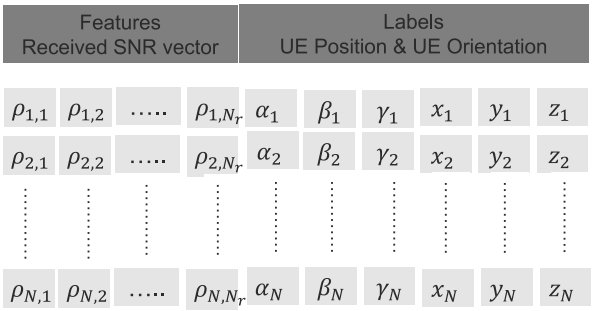

(a) Position and Orientation estimation Dataset

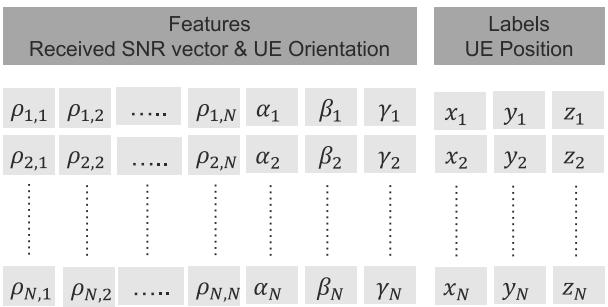

(b) Orientation-aided positioning Dataset

FIGURE 5. Dataset Structure.

a complete CNN can be formed. The input layer initiates the neural network, receiving the feature vector ρ and the bias parameter b_1 as inputs. The Dth hidden layer typically comprises convolutional layers, ReLU layers and pooling layers, where each dth layer, for $d \in [1, D]$, can be considered as consisting of M_d neuron units. The neurons with each dth layer interconnected with the neurons in the $d+1$th layer to form a neural network. After traversing the D layers of hidden units, the output progresses to the FC layer for final classification. The FC layer plays the role of "classifier" in the whole CNN. If the operations of convolutional layer, pooling layer and activation function are to map the original data to the hidden layer feature space (the process of feature extraction and selection), the FC layer plays the role of mapping the learned feature representation to the label vectors of the samples. In other words, it is to integrate the features together (highly purified features) to facilitate handing over to the final classifier or regression. Thus, it outputs the 3D position and 3D orientation parameters of the UEs.

The convolutional layers of this network, which increase exponentially in the number of filters or neurons, enable the network to progressively extract a broader and more complex range of features. Early layers focus on simpler features like edges or basic textures, while subsequent layers address more complex structures critical for detailed recognition tasks. Employing a small kernel size throughout these layers balances spatial resolution with feature extraction capability, preserving essential details.

ReLU activation is employed throughout the layers to compute non-linearity efficiently, reduce computational load, and prevent the vanishing gradient problem, where gradients diminish during backpropagation, can stall the learning process in deep learning models. The network transitions from feature extraction to synthesis in the fully connected layers, which feature a large number of neurons to integrate the extracted features. This integration enables the network to learn from a vast feature set and identify intricate patterns necessary for final predictions. While ReLU is used predominantly, the final layer employs a linear activation function suitable for numerical outputs as in regression models or specific classifications.

The Mean Squared Error (MSE) serves as the loss function to refine and enhance the network's predictive accuracy, making it a tool in scenarios demanding high precision in continuous numerical forecasts. The MSE quantifies the average squared discrepancies between predicted values ($\hat{y}_i$) and observed actual values (y_i), as defined by the following equation:

$$\text{Loss} = \frac{1}{n}\sum_{i=1}^{n}\left(\hat{y}_i - y_i\right)^2 \tag{9}$$

This expression underscores the squaring of prediction errors, averaged across all data points, and is applied in regression analyses to enhance prediction accuracy by minimizing MSE throughout the training of machine learning models. Here, n represents the quantity of datasets employed in the training and validation stages. Specifically, in a dataset focused on the estimation of position and orientation, $\hat{y}_i$ and y_i in the equation denote the normalised estimated and actual values of position and orientation $(x, y, z, \alpha, \beta, \gamma)$, respectively. In addition, for the orientation-aided positioning dataset, $\hat{y}_i$ and y_i refer to the normalised predicted and actual positions (x, y, z).

Following the implementation and training of the CNN models, optimal parameters are determined. The system then transitions to the testing phase. SNR values are measured at the APs on the ceiling, alongside UE information, are input into the trained model, which then estimates the required information. The UEs are connected to at least one AP at any time which indicates that the links between the APs and UEs are activated. Having only one non-zero link suggests that the UE is close to the corresponding AP and oriented towards it. Upon detecting new SNR values, the trained CNN model processes these values to estimate the UE's 3D position.

IV. SIMULATION RESULTS

A. SIMULATION PARAMETERS

Parameters for the typical indoor LiFi system are set as $L \times W \times H_{\text{room}} = 5 \times 5 \times 3$ m^3. In order to compare the positioning performance of multi-directional with single-directional structures, the number of APs chosen is the same as in [18], i.e., $N_{\text{r}} = 16$. These APs are arranged in a 4×4 array, each one metre apart, centrally placed on the

TABLE 2. Basic LiFi system simulation parameters.

Parameter	symbol	actual value
Room size	$L \times W \times H_{\text{room}}$	$5m \times 5\text{m} \times 3\text{m}$
LED half-power semiangle	$\Phi_{1/2}$	$60°$
PD responsivity	R_p	0.6 A/W
single PD size	A_g	1cm^2
Maximum UE's height	H_{device}	1.5 m
Maximum UE's power	$P^m_{elec}ax$	0.01 W
Reflection index of the wall	ζ	0.7
PDs FOV	Ψ	90 °
System bandwidth	B	10 MHz
Noise power spectral density	N_0	10^{-21}W/Hz

TABLE 3. Current CNN for the multi-directional structure.

Layers	No. of Filters/Neurons	Filter size	Activation Function	Padding
Con1D No.1	8	2	ReLU	None
Con1D No.2	16	2	ReLU	None
Con1D No.3	32	2	ReLU	None
Con1D No.4	64	2	ReLU	None
Con1D No.5	128	2	ReLU	None
Con1D No.6	256	2	ReLU	None
FC layers-1	4096 Neurons	-	ReLU	-
FC layers-2	4096 Neurons	-	ReLU	-
FC layers-3	n-outputs(6)	-	Linear	-

square ceiling and oriented vertically downwards. The size of the UE mimics a standard mobile phone, measuring $14 \times 7 \times 1$ cm [19]. For the single-directional structure, the LED is positioned 6 cm above the center of mobile phone. For the multi-directional structure, the PD associated with n_3 is placed at the center of the corresponding side, and the PDs indicates by n_2 and n_4 are positioned 1.5 cm from the top edge. Other relevant simulation parameters are presented in the Table 2.

B. CNN PARAMETERS AND SPECIFICATION

The architecture of the proposed CNN is detailed in Table 3. This CNN network consists of 1 input layer, 6 convolution layers and 3 FC layers. In the convolutional layers, filter and stride size are respectively 2 and 1, with the number of filters increasing exponentially from 8 to 256. The first two FC layers have 4096 neurons each, while the third layer serves as a dropout layer with 6 outputs. There are two datasets considered for the current CNN input, which have the size of $N = 10^5$ and $N = 10^6$ points. Moreover, for each dataset size N, the $0.9 \times N$ points are used for training the CNN model, and the remainder for testing. In terms of CNN structure, the CNN in [18] consists of 4 hidden layers with 256 neurons per layer and 64 filters. However, the current CNN employs an increasing number of filters per convolutional layer, which captures a more detailed hierarchy of features, particularly beneficial for complex pattern recognition tasks. While the previous CNN used a kernel size of 16, the current CNN uses smaller kernel sizes like 2x2 across all convolutional layers,

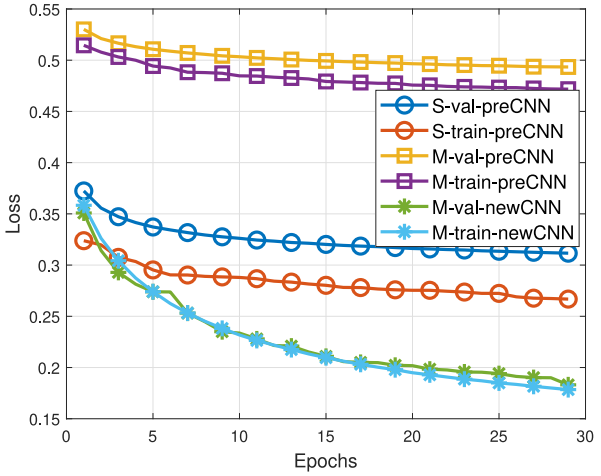

FIGURE 6. Comparative analysis of single-directional (S) and multi-directional (M) structures in positioning performance: previous CNN (preCNN) vs. current work (newCNN) in train and validation (val) phase.

allowing for finer granularity in feature extraction. More importantly, we introduced a brand new orientation-aided dataset as input, providing additional and more accurate features to the CNN. Overall, a more effective CNN structure and refined datasets have led to a significant improvement in positioning accuracy.

C. POSITION AND ORIENTATION ESTIMATION

We first evaluated the new MDT datasets using the model from [18], which apply the CNN model with 4 1D convolution layers, 4 normalization layers and 4 dropout layers, combining with 64 filters in each convolution layer. The loss function is Mean-Squared-Error (MSE), and the loss trend is shown in Fig. 6. This figure presents the estimated loss by MSE against the epoch index over a total of 30 epochs for both training and validation processes. It can be seen that the performance for MDT is degraded, despite having multiple transmitters in different directions, compared to the single-directional structure when the same CNN model in [18] used. The new CNN in Table 3 enables MDT to produce a better performance. Utilizing the new CNN, the loss trend is also denoted in Fig. 6. The results reveal that the new CNN network yields significantly lower losses than the previous model, both in training and validation. With a dataset size of $N = 10^6$, training and validation losses are approximately 18%, which is a notable improvement.

Accuracy is a commonly used metric to assess the performance of classification models. The calculation of accuracy is relatively straightforward, primarily measuring the ratio of the number of samples correctly predicted by the model to the total number of samples. However, the calculation of the accuracy rate in this system addresses a complex classification problem, necessitating the introduction of a threshold. The formula for calculating the accuracy rate is as follows:

$$\text{Accuracy} = \frac{\text{Number of accurate estimations}}{\text{Total number of estimations}} \tag{10}$$

An accurate estimation is defined as an estimation where the Euclidean Distance error is less than or equal to the accepted error, denoted as ϵ, which is measured in meters, determining the allowable distance from the actual position that can still be considered an accurate estimation. In this study, we employ the default parameter value for the Adam optimizer, set at 10^{-7}m.

Although the new network was able to reduce the loss to less than 20%, the model achieved an accuracy of only 70% in estimating position and orientation. In order to evaluate which parameter is responsible for the poor accuracy performance, the Cumulative Distribution Function (CDF) is introduced for position error and orientation error in yaw, pitch and roll angles, respectively. The position and orientation error samples can be calculated as follows: position error $=|$ (estimated position $-$ exact position) $|$; orientation error $=|$ (estimated angles $-$ exact angles) $|$. The CDFs of the position and orientation error are shown in the Fig. 7.

According to the CDF, it is evident that the yaw angle exerts the most significant influence on the overall estimation accuracy, whereas the 80% position errors are below 10cm, pitch and roll angle errors are under 2°. Importantly, for the positioning system, the accuracy of the position information (x, y, z) is paramount. Given the improving accuracy of device sensors in measuring the orientation angle of the UE, it is feasible to utilize the angle measured by the phone's sensor, along with the SNR vector, as feature vectors. Consequently, the position (x, y, z) can be exclusively used as the label. Note that the availability of the orientation data is an assumption for specific scenarios, such as smartphones, which may not be applicable to other use cases. This approach may enhance the performance of the CNN. The following section presents the process and results.

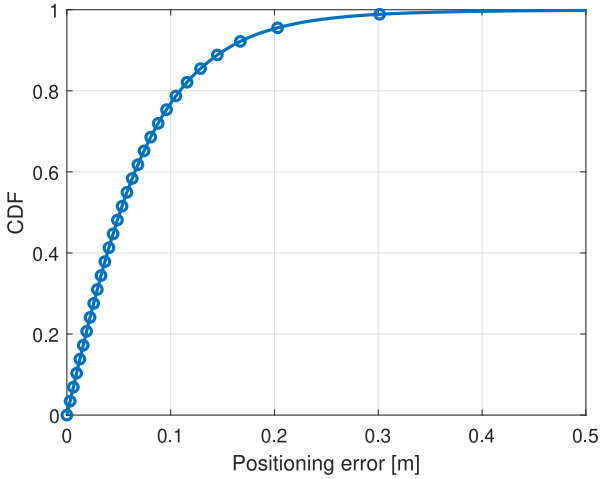

(a) position error CDF

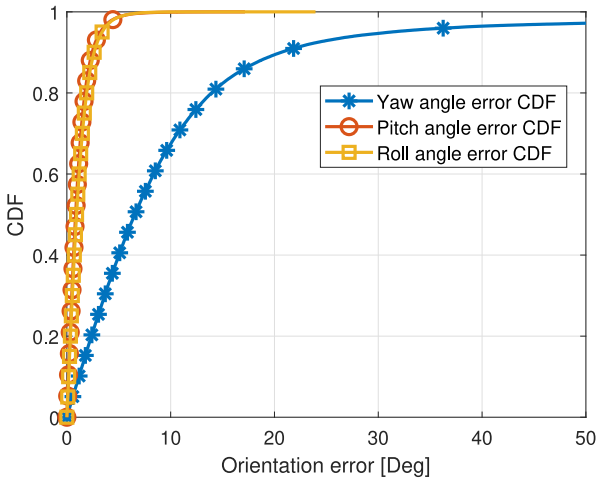

(b) orientation angle error CDF

FIGURE 7. CDF of position and orientation error for simultaneous position and orientation estimation.

D. ORIENTATION-AIDED POSITIONING

1) NOISE-FREE POSITION ESTIMATION

We use the Orientation-aided positioning dataset and assume that the measured orientation data are accurate. With this assumption, the parameters of the model remain largely unchanged, except for the modification of the FC layer in the final CNN layer, which should be configured to produce an output vector with a size of 3. The input dataset structure, on the other hand, is as shown in the Fig. 5(b), where orientation dataset is generated by the exact data without measurement noise. The datasets are available in two sizes, with $N = 10^5$ and $N = 10^6$ respectively. The performance of the proposed CNN using Orientation-aided positioning, are illustrated in Fig. 8. In the Fig. 8(a), the training and validation loss for the dataset sizes of $N = 10^5$ and $N = 10^6$ have decreased to the 1% and 0.5%, respectively, representing a dramatic improvement compared to the previous results using the position and orientation estimation dataset, 17%, shown in the Fig. 6. Concurrently, the accuracy of both the training and validation datasets has improved to approximately 96% and 98%. These results suggest that considering orientation as a feature vector contributes positively to the accuracy of position estimation.

2) IMPACT OF DISTRIBUTION OF APS

In real-time applications, having 16 LEDs on the ceiling may be excessive for a single room, necessitating a re-evaluation of the number of LEDs and the impact of APs in the current system. As illustrated in the Fig. 9, we modify the distribution and quantity of APs to the following configuration. For the training of the CNN model, datasets of varying sizes, specifically $N = 10^5$ and $N = 10^6$, are utilized to accommodate the differences in AP distributions. The outcomes of this approach are illustrated in the Fig. 10.

As expected, a lower number of APs corresponds to a reduction of accuracy. Furthermore, the CNN model encounters a bottleneck when the number of APs is reduced to four where the validation loss and accuracy saturated, despite the continuously decreasing and increasing in the training loss and accuracy separately, as depicted in Fig. 10(a) and 10(b).

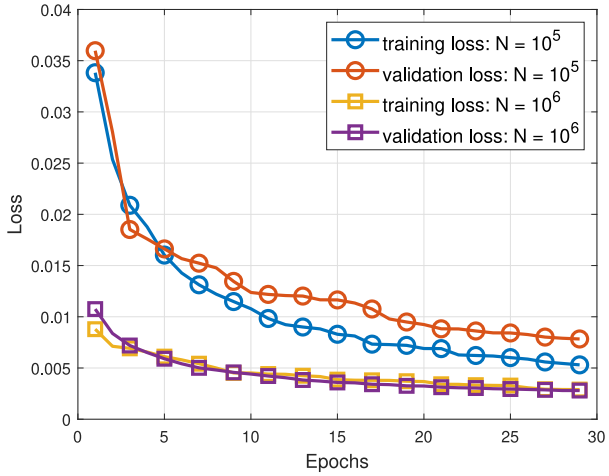

(a) Loss(MSE) of estimation 3D position

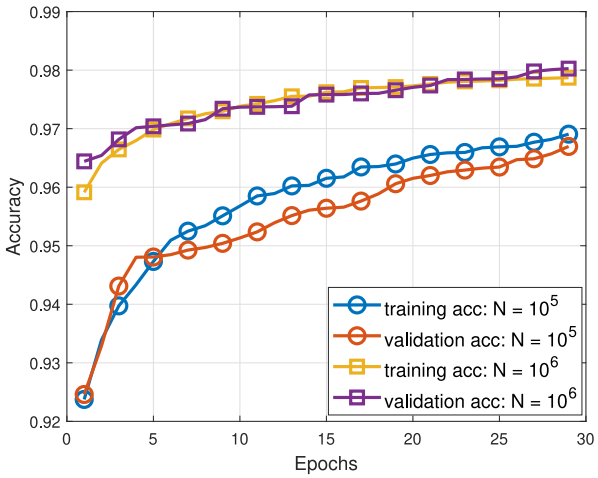

(b) Accuracy of estimation 3D position

FIGURE 8. Loss and accuracy of estimation of position using orientation-aided positioning.

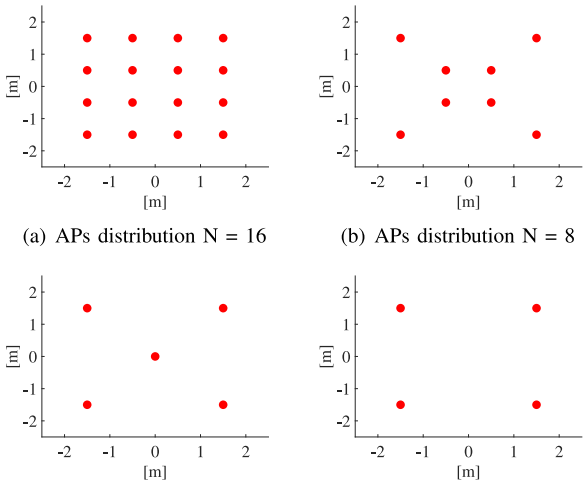

(a) APs distribution N = 16 (b) APs distribution N = 8

(c) APs distribution N = 5 (d) APs distribution N = 4

FIGURE 9. Different numbers and distributions of APs.

TABLE 4. Average estimation 3D position error.

N	Estimation error (cm)	Dataset size $N = 10^5$			Dataset size $N = 10^6$		
		exact	noisy	NR	exact	noisy	NR
16	mean	5.55	6.27	5.87	1.81	3.20	2.31
	precision	8.45	9.32	9.08	6.32	7.65	7.03
8	mean	6.73	7.08	6.87	3.11	4.50	3.57
	precision	9.34	10.54	10.02	7.83	8.64	8.26
5	mean	8.50	9.09	8.77	5.36	7.12	5.89
	precision	10.21	12.32	11.56	8.92	10.34	9.63
4	mean	saturation	saturation	saturation	6.38	9.12	7.15
	precision	saturation	saturation	saturation	10.12	12.39	12.03

This phenomenon can be attributed to the fact that a reduction in the number of LEDs leads to a corresponding decrease in the quantity of features that the CNN can extract, consequently resulting in the saturation of its processing capacity. In contrast, expanding the dataset size to $N = 10^6$, the proposed CNN can reduce the MSE loss to 1.5% accompanied by 95% accuracy with just 4 LEDs.

3) POSITION ESTIMATION CONSIDERING NOISE AND WITH NOISE REDUCTION

In order to match the system with practical scenarios, it is necessary to introduce noise into the orientation dataset. Based on the data from [2], the error in rotation angles measured by the mobile phone sensors can be approximated as standard deviation of 2.2°. Therefore, random Gaussian white noise with standard deviation of 2.2° was added to the generated 3D orientation dataset used as the sensor measurement, while other parameters remained unchanged. The evaluation results show the impact of the sensor noise in Table 4. This implies the need for algorithms to minimize the effect of noise on estimation results.

We develop a noise reduction (NR) algorithm by efficiently using the rotation angles estimated by the proposed CNN network, sensor measured rotation angles, and exact values. This creates a new orientation dataset less influenced by noise for the training phase. Meanwhile, the measured rotation angles with noise are used for the testing phase. In this algorithm, θ_{measured} denotes the rotation angles $\theta(\alpha, \beta, \gamma)$ ascertained via the mobile device's sensor system, while $\theta_{\text{estimated}}$ refers to the rotation angles estimated through the Position and Orientation estimation Estimation approach. The term θ_{exact} is used to represent the exact yaw, pitch and yaw angles. The algorithm calculates the minimum error among e_i, $i = 1, 2, 3$, by comparing differences between the estimated and exact rotation angles, the measured and exact rotation angles, as well as the average of the measured and estimated rotation angles with the exact values. When i represents the index of the smallest value among e_1, e_2, and e_3, the new rotation angle θ_i is updated to θ. This process facilitates the generation of a refined dataset for orientation angles for training CNN model. According to the analysis during training, 62.75% of the new rotation angles were angles measured by the device sensor, while the

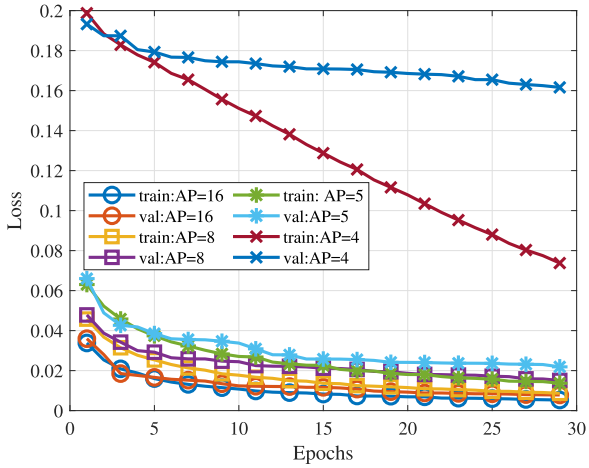

(a) Loss for different APs distribution $N = 10^5$

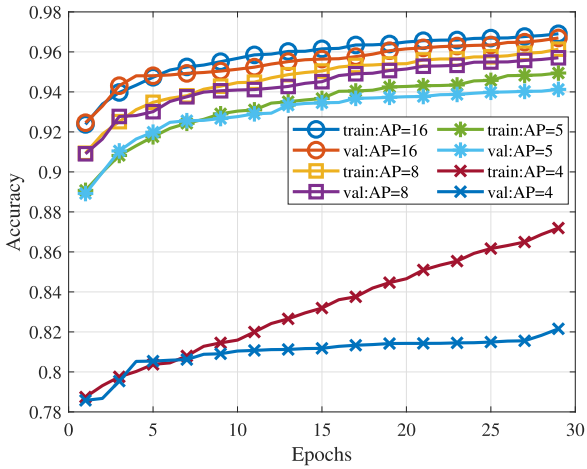

(b) Accuracy for different APs distribution $N = 10^5$

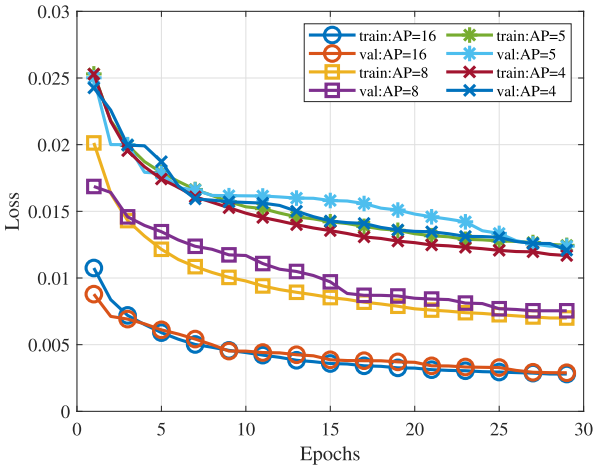

(c) Loss for different APs distribution $N = 10^6$

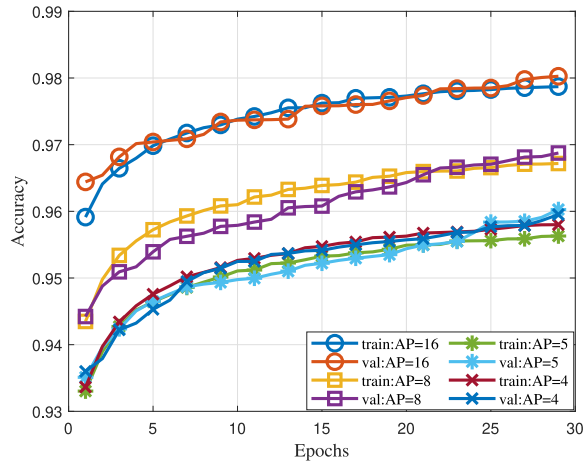

(d) Accuracy for different APs distribution $N = 10^6$

FIGURE 10. The performance of the orientation aided positioning with different APs distribution.

average angles as well as the estimated angles were 23.62% and 13.63%, respectively. Thus, it can be inferred that the use of the noise reduction algorithm helps when training a model without the effect of noisy outlier data or highly inaccurate estimation, helping to improve the accuracy of the positioning for the testing phase.

The results for the estimation error for the testing phase are shown in the Table 4. The use of the NR represents a substantial enhancement of localisation accuracy even in the presence of noise. Two further metrics are considered to present the overall performance of different methods of this paper: Average position error is calculated as the mean of estimation errors for x, y, and z coordinates. The precision of position error is defined as the positioning error at the 80 percentile of CDF, denoted as $\text{Precision}_{\text{Position error}} = \text{Positioning error}_{\text{at 80\% CDF}}$. The average position error and precision according to the number of LED and the size of the dataset is shown in Table 4.

In fact, the reduction of number of LEDs leads to a larger average error. Additionally, noise becomes a significant factor when using phone sensors to measure orientation. However, the noise reduction algorithm demonstrates effective performance, substantially decreasing the position error in all cases. For $N = 10^6$, the CDFs for various APs distributions are shown in Fig. 11. When analyzing the dataset size of $N = 10^6$ with 16 APs on the ceiling, the proposed CNN model achieves an average position error of 1.81 cm in an exact case and 2.42 cm with noise. In [18], using MLP and ANN with position and orientation estimation datasets ($N = 10^6$) as inputs, the minimal errors in position estimation were recorded at 13.04 cm and 10.53 cm, respectively. The proposed CNN illustrates a significant improvement. As the number of LEDs reduces, the average position error reaches a maximum of 7.25 cm with NR, which is still an acceptable performance for many scenarios.

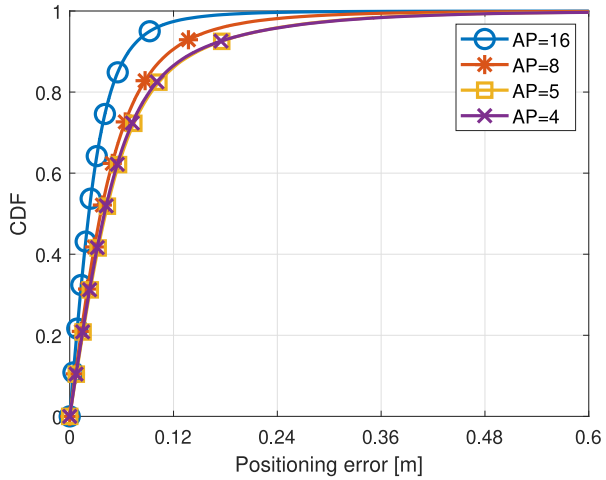

FIGURE 11. CDFs of positioning error for different APs distribution at $N = 10^6$.

Algorithm 1 Computing the New Rotation Angles Datasets

$\theta_1 = \theta_{\text{measured}}$
$\theta_2 = \theta_{\text{estimated}}$
$\theta_3 = \frac{(\theta_{\text{measured}} + \theta_{\text{estimated}})}{2}$
$e_1 = \mid (\theta_{\text{estimated}} - \theta_{\text{exact}}) \mid$
$e_2 = \mid (\theta_{\text{measured}} - \theta_{\text{exact}}) \mid$
$e_3 = \mid (\frac{(\theta_{\text{measured}} + \theta_{\text{estimated}})}{2} - \theta_{\text{exact}}) \mid$
$i = \arg\min(e_1, e_2, e_3)$
$\theta = \theta_i$

V. CONCLUSION

In this paper, a new CNN model has been introduced for an accurate positioning for an OWC system to compensate for the limitation of previous models that focused solely on single-directional transceiver structures. The proposed model is tailored for joint 3D position and orientation estimation. We further refined the model to consider only position as the label, with feature vectors comprising SNR vectors and measured orientation data. This modification enabled the CNN models to achieve an average position error of below 2 cm. We also incorporated noise into the orientation angles typically observed in sensor measurements. We employed a noise reduction algorithm to keep the average estimation error around 2 cm. The impact of number of APs was studied. It was demonstrated that even with 4 APs, average errors as low as 7.25 cm can be achieved. Overall, these results suggest a viable approach for achieving highly accurate position estimation. Experimental evaluation of this approach will be completed and presented in a later work.

ACKNOWLEDGMENT

The authors greatly appreciate Dr. Amlan Basu's insightful discussion during this research.

REFERENCES

[1] P. Escaleira, V. A. Cunha, D. Gomes, J. P. Barraca, and R. L. Aguiar, "Moving target defense for the cloud/edge Telco environments," *Internet Things*, vol. 24, Dec. 2023, Art. no. 100916.

[2] "Estimate phone orientation using sensor fusion." MATLAB. May 2021. [Online]. Available: https://uk.mathworks.com/help/nav/ug/estimate-phone-orientation-using-sensor-fusion.html

[3] J. M. Dow, R. E. Neilan, and C. Rizos, "The international GNSS service in a changing landscape of global navigation satellite systems," *J. Geodesy*, vol. 83, pp. 191–198, Mar. 2009.

[4] C. J. Hegarty and E. Chatre, "Evolution of the global navigation satellitesystem (GNSS)," *Proc. IEEE*, vol. 96, no. 12, pp. 1902–1917, Dec. 2008.

[5] H. Lan, C. Yu, Y. Zhuang, Y. Li, and N. El-Sheimy, "A novel Kalman filter with state constraint approach for the integration of multiple pedestrian navigation systems," *Micromachines*, vol. 6, no. 7, pp. 926–952, 2015.

[6] Y. Zhuang and N. El-Sheimy, "Tightly-coupled integration of Wi-Fi and MEMS sensors on handheld devices for indoor pedestrian navigation," *IEEE Sensors J.*, vol. 16, no. 1, pp. 224–234, Jan. 2015.

[7] S. E. Trevlakis et al., "Localization as a key enabler of 6G wireless systems: A comprehensive survey and an outlook," *IEEE Open J. Commun. Soc.*, vol. 4, pp. 2733–2801, 2023.

[8] M. D. Soltani et al., "Terabit indoor laser-based wireless communications: LiFi 2.0 for 6G," *IEEE Wireless Commun.*, vol. 30, no. 5, pp. 36–43, Oct. 2023.

[9] U. Sen, Y. E. Yesilirmak, I. O. Bayman, T. Arsan, E. Panayirci, and N. Stevens, "3D indoor positioning with spatial modulation for visible light communications," *Opt. Commun.*, vol. 529, Feb. 2023, Art. no. 129091. [Online]. Available: https://www.sciencedirect.com/science/article/pii/S0030401822007386

[10] P. Du, S. Zhang, C. Chen, A. Alphones, and W.-D. Zhong, "Demonstration of a low-complexity indoor visible light positioning system using an enhanced TDOA scheme," *IEEE Photon. J.*, vol. 10, no. 4, pp. 1–10, Aug. 2018.

[11] S. Shen et al., "Hybrid position and orientation estimation for visible light systems in the presence of prior information on the orientation," *IEEE Trans. Commun.*, vol. 21, no. 8, pp. 6271–6284, Aug. 2022.

[12] H.-S. Kim et al., "An indoor visible light communication positioning system using a RF carrier allocation technique," *J. Lightw. Technol.*, vol. 31, no. 1, pp. 134–144, Jan. 1, 2012.

[13] J. Lim, "Ubiquitous 3D positioning systems by LED-based visible light communications," *IEEE Wireless Commun.*, vol. 22, no. 2, pp. 80–85, Apr. 2015.

[14] M. T. Van, N. Van Tuan, T. T. Son, H. Le-Minh, and A. Burton, "Weighted K-nearest neighbour model for indoor VLC positioning," *Inst. Eng. Technol. Commun.*, vol. 11, no. 6, pp. 864–871, 2017.

[15] A. Gradim, P. Fonseca, L. N. Alves, and R. E. Mohamed, "On the usage of machine learning techniques to improve position accuracy in visible light positioning systems," in *Proc. 11th Int. Symp. Commun. Syst., Netw. Digit. Signal Process. (CSNDSP)*, 2018, pp. 1–6.

[16] X. Li, Y. Cao, and C. Chen, "Machine learning based high accuracy indoor visible light location algorithm," in *Proc. IEEE Int. Conf. Smart Internet Things (SmartIoT)*, 2018, pp. 198–203.

[17] J. He et al., "Demonstration of high precision 3D indoor positioning system based on two-layer ANN machine learning technique," in *Proc. Opt. Fiber Commun. Conf. Exhibit. (OFC)*, 2019, pp. 1–3.

[18] M. A. Arfaoui et al., "Invoking deep learning for joint estimation of indoor LiFi user position and orientation," *IEEE J. Sel. Areas Commun.*, vol. 39, no. 9, pp. 2890–2905, Sep. 2021.

[19] M. D. Soltani et al., "Bidirectional optical spatial modulation for mobile users: Toward a practical design for LiFi systems," *IEEE J. Sel. Areas Commun.*, vol. 37, no. 9, pp. 2069–2086, Sep. 2019.

[20] "Light antenna ONE." pureLiFi. 2024. Accessed: May 12, 2024. [Online]. Available: https://www.purelifi.com/products/light-antenna-one/

[21] H. Schulze, "Frequency-domain simulation of the indoor wireless optical communication channel," *IEEE Trans. Commun.*, vol. 64, no. 6, pp. 2551–2562, Jun. 2016.

[22] M. D. Soltani, A. A. Purwita, Z. Zeng, H. Haas, and M. Safari, "Modeling the random orientation of mobile devices: Measurement, analysis and LiFi use case," *IEEE Trans. Commun.*, vol. 67, no. 3, pp. 2157–2172, Mar. 2019.

YIFAN HUANG received the M.Sc. degree (with Distinction) in electrical and electronic engineering from the University of Strathclyde in 2022, where he is currently pursuing the Ph.D. degree, focusing on optical wireless technologies, specifically Visible Light Positioning. He has actively participated in significant academic activities, including the IEEE Wireless Communications and Networking Conference in 2023 and the 49th European Conference on Optical Communications in 2023.

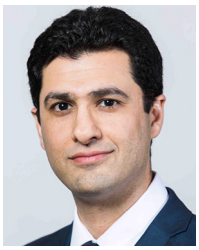

MAJID SAFARI (Senior Member, IEEE) received the Ph.D. degree in electrical and computer engineering from the University of Waterloo, Canada, in 2011. He is currently a Professor of Optical and Wireless Communications and the Deputy Head of the Institute for Imaging, Data, and Communications, The University of Edinburgh. He has published more than 150 papers. He is a recipient of prestigious grants from Leverhulme Trust and EPSRC, U.K. His main research interests include the application of optics, information theory, and signal processing in optical, wireless, and quantum communications. He is a recipient of Mitacs Fellowship, Canada. He received Best Paper Awards from IEEE GLOBECOM 2022 and IEEE ICC 2023. He is an Associate Editor of IEEE TRANSACTIONS ON COMMUNICATIONS. He was also an Associate Editor of IEEE COMMUNICATION LETTERS from 2015 to 2019, and served as the TPC Co-Chair of the 4th Workshop on Optical Wireless Communication (IWOW) in 2015 and the OWC Workshop at IEEE WCNC 2023.

HARALD HAAS (Fellow, IEEE) received the Ph.D. degree from The University of Edinburgh, Edinburgh, U.K., in 2001. He is currently the Van Eck Professor of Engineering with the University of Cambridge and the Director of the LiFi Research and Development Centre. He founded pureLiFi Ltd. and holds the position of a Chief Scientific Officer. He has co-authored more than 650 conference and journal papers with more than 55 000 citations and holds more than 45 patents. His most recent research interests lie in integrating physics and communication theory to design secure, high-speed wireless multiuser access networks, and distributed x-haul networks utilizing the optical spectrum toward building net-zero and pervasive wireless networks. In 2016, he was the recipient of the Outstanding Achievement Award from the International Solid State Lighting Alliance. He was awarded a Royal Society Wolfson Research Merit Award in 2017. In 2019, he received the IEEE Vehicular Society James Evans Avant Garde Award and the Enginuity The Connect Places Innovation Award in 2021. In 2022, he was the recipient of the Humboldt Research Award for his research achievements. In 2023, he among the three shortlisted candidates for a European Inventor Award. He has been listed as a Highly Cited Researcher by Clarivate/Web of Science since 2017. He has delivered two TED talks and one TEDx talk which have been watched online more than 5.5 million times. He is a Fellow of the Royal Academy of Engineering, of the Royal Society of Edinburgh, and of the Institution of Engineering and Technology.

IMAN TAVAKKOLNIA (Member, IEEE) received the Ph.D. degree from The University of Edinburgh in 2018. He is an Assistant Professor with the Electrical Engineering Division, University of Cambridge, U.K. He was a Research Associate with The University of Edinburgh until 2020, and then with the University of Strathclyde until September 2021, before being appointed as a Strathclyde Chancellor's Fellow (Lecturer) until February 2024. He is a co-investigator on two EPSRC Future Communication Hubs in the U.K. (TITAN EP/X04047X/1 and HASC EP/X040569/1) as well as the £12M Future Open Networks Research Challenge Grant funded by the U.K.'s Department of Science, Innovation and Technology. His research focuses on developing a fundamental understanding of the energy-efficiency of current and future telecommunication systems and lies on the frontier of communication theory, advanced materials, signal processing, and optical communications. He is an Associate Editor of the IEEE COMMUNICATIONS LETTERS. He has been a Co-Chair of the Optical Wireless Communication Workshops in WCNC 2023 and 2024, a Local Organizing Committee Member of ECOC 2023, and a TPC member of several workshops and conferences. He is a working Group Member of the European COST Action and CA19111 NEWFOCUS.